

A numerical study of the spectrum and eigenfunctions on a tubular arc

Lonnie Mott, Mario Encinosa, and Babak Etemadi

Department of Physics
Florida A & M University
Tallahassee, Florida 32307

Abstract

The Hamiltonian for a particle constrained to move on the surface of a curved nanotube is derived using the methods of differential forms. A two-dimensional Gram-Schmidt orthonormalization procedure is employed to calculate basis functions for determining the eigenvalues and eigenstates of a tubular arc (a nanotube in the shape of a hyperbolic cosine) with several hundred scattering centers. The curvature of the tube is shown to induce bound states that are dependent on the curvature parameters and bend location of the tube.

PACS number(s): 03.65.Ge, 68.65.-k

Keywords: curved nanotubes, constrained systems

1. Introduction

The quantum mechanics of reduced dimensionality systems [1-7] has become a subject of importance in modelling devices for which the geometric properties of the device become a factor in influencing its behavior [8-15]. Carbon nanotubes are such objects; the electronic properties of straight nanotubes are determined primarily by the chirality of the tubes and are well understood [16]. However, bent, curved, and toroidal CNT's have been observed [17], and their potential application as device elements makes it necessary to model such structures as well.

In this paper we perform a curved manifold Schrodinger equation calculation to determine the spectrum and eigenfunctions for a particle constrained to move on the surface of a curved nanotube with delta function site potentials. The methods of differential forms are used to derive the Hamiltonian of a particle constrained to move on the surface of a curved nanotube. Initially the particle is taken to be in three-dimensional space; it is then confined to move on a two-dimensional curved manifold by a potential everywhere normal to the surface. This reduction in dimensionality yields a curvature-dependent potential V_D [1-7,18-20] that is added to the Hamiltonian. Then, using a hyperbolic cosine shape function, the eigenvalues and eigenvectors for the low-lying states of a tubular arc with and without δ -function potentials are calculated with a basis set expansion wherein a two-dimensional Gram-Schmidt procedure is employed to build the basis states.

The remainder of this paper is organized as follows: in section 2 the method used to derive the Hamiltonian is explained in detail. In section 3, a brief overview of the model used for

the tubular arc is given. A periodic delta function potential is also introduced to mimic atomic sites or defects. In section 4 the method used to solve the Hamiltonian derived in section 2 is briefly described. Results for the eigenvectors and eigenvalues of the arc without delta functions, as well as the lowest energy eigenvalues with delta sites, are presented. The conclusions are given in section 5.

2. Derivation of the Hamiltonian

Consider a quantum particle in the neighborhood of a two-dimensional manifold Σ imbedded in R^3 . Any point in the neighborhood of Σ can be given by the Monge form plus a normal term

$$\vec{r}(q_1, q_2, q_3) = \vec{x}(q_1, q_2) + q_3 \hat{e}_3 \quad (1)$$

where \vec{x} describes the manifold, and \hat{e}_3 is the unit vector normal to the surface. Applying the exterior derivative operator [21] d gives the one-form

$$d\vec{r} = d\vec{x} + dq_3 \hat{e}_3 + q_3 d\hat{e}_3 \quad (2)$$

where dq_3 is the incremental displacement along the normal to the surface. $d\vec{x}$ lies in the tangent plane and is given by

$$d\vec{x} = \sigma_1 \hat{e}_1 + \sigma_2 \hat{e}_2 \quad (3)$$

\hat{e}_1 and \hat{e}_2 are locally orthonormal unit vectors tangent to the surface; σ_1 and σ_2 are one-forms on Σ . The exterior derivative of any zero-form (scalar function) ψ in the neighborhood of Σ is given by

$$d\psi = \frac{\partial\psi}{\partial q_1} dq_1 + \frac{\partial\psi}{\partial q_2} dq_2 + \frac{\partial\psi}{\partial q_3} dq_3 = \nu_1 \tau_1 + \nu_2 \tau_2 + \nu_3 dq_3 \quad (4)$$

ν_1 , ν_2 , and ν_3 are zero-form functions and τ_1 , τ_2 , and dq_3 are the one-forms in the neighborhood of the surface Σ .

Applying the Hodge * operator to the one-form of Eq. (4) gives

$$*d\psi = \nu_1 \tau_2 dq_3 + \nu_2 dq_3 \tau_1 + \nu_3 \tau_1 \tau_2 \quad (5)$$

A second application of the exterior derivative operator yields

$$d * d\psi = (\Delta\psi) \tau_1 \tau_2 dq_3 \quad (6)$$

where Δ is the Laplace-Beltrami operator. The time independent Schrodinger equation becomes

$$-\frac{\hbar^2}{2m^*} \Delta\psi(\vec{r}) + V(\vec{r})\psi(\vec{r}) = E\psi(\vec{r}) \quad (7)$$

In the development above, no constraint has been imposed on the particle. To bring the particle to the surface, we imagine an oscillator potential $V(q_3) = \frac{1}{2}m^* \varpi^2 q_3^2$ everywhere

normal to Σ acting to enforce the condition that the particle remains in the neighborhood of Σ . In the limit that $\varpi \rightarrow \infty$, then $q_3 \rightarrow 0$. However, it is not enough simply to include this term in Eq. (7); to preserve the norm as the particle approaches the surface, it must further hold that for $q_3 \rightarrow 0$ [2,3,4]

$$|\psi(q_1, q_2, q_3)|^2 F dS dq_3 \rightarrow |\chi(q_1, q_2, q_3)|^2 dS dq_3 \quad (8)$$

which allows the identification

$$\psi = \frac{\chi}{\sqrt{F}} \quad (9)$$

where

$$F = 1 + 2q_3 H + q_3^2 K$$

H and K are the mean and Gauss curvatures respectively and only depend on the surface coordinates q_1 and q_2 . Performing the standard factorization of χ into tangential and normal parts and taking the $q_3 \rightarrow 0$ limit gives two equations when Eq. (9) is substituted into Eq. (7),

$$-\frac{\hbar^2}{2m^*} \Delta_t \Psi - \frac{\hbar^2}{2m^*} (H^2 - K) \Psi = \varepsilon \Psi \quad (10)$$

and

$$-\frac{\hbar^2}{2m^*} \frac{\partial^2 \Phi}{\partial q_3^2} + V(q_3) \Phi = \epsilon \Phi \quad (11)$$

The derivative free term in Eq. (10) is the distortion potential V_D , dependent on the mean curvature H and the Gauss curvature K of the surface

$$V_D(q_1, q_2) = -\frac{\hbar^2}{2m^*} (H^2 - K) \quad (12)$$

It should be noted that V_D is not necessarily the only modification to the Laplace-Beltrami operator. Even for surfaces possessing symmetry, factors related to the metric can appear in the kinetic-energy operator and in general cannot be transformed away [22].

To apply the formalism described above to nanotubes, consider a tube of radius a and let u be the coordinate axis along \hat{i} . The surface of the tube can be described by

$$\vec{x}(\theta, u) = (u - a\beta \cos \theta) \hat{i} + (f(u) + a\alpha \cos \theta) \hat{j} + (a \sin \theta) \hat{k} \quad (13)$$

where $f(u)$ is the shape function for the axis of the tube, $\alpha = (1 + f_u^2)^{-1/2}$, $\beta = (1 + f_u^2)^{-1/2} f_u$, and $f_u = \partial_u f(u)$. Applying d to Eq. (13) and using Eq. (3), we find that

$$\sigma_1 = a d\theta \quad (14a)$$

$$\sigma_2 = \lambda(\theta, s) ds \quad (14b)$$

and

$$\hat{e}_1 = \beta(s) \sin \theta \hat{i} - \alpha(s) \sin \theta \hat{j} + \cos \theta \hat{k} \quad (15a)$$

$$\hat{e}_2 = \alpha(s) \hat{i} + \beta(s) \hat{j} \quad (15b)$$

$$\hat{e}_3 = -\beta(s) \cos \theta \hat{i} + \alpha(s) \cos \theta \hat{j} + \sin \theta \hat{k} \quad (15c)$$

with the integration measure, axis curvature, and arclength given by $\lambda(\theta, s) = 1 - a\kappa(s) \cos \theta$, $\kappa = (1 + f_u^2)^{-3/2} f_{uu}$, and $ds = \sqrt{1 + f_u^2} du$, respectively. Any point in the neighborhood of the tube is given by Eq. (1). The Laplace-Beltrami operator can thus be written

$$\Delta = \frac{1}{\mu^2} \left(\frac{\partial^2}{\partial \theta^2} + \frac{\partial \ln \Lambda}{\partial \theta} \frac{\partial}{\partial \theta} \right) + \frac{1}{\Lambda^2} \left(\frac{\partial^2}{\partial s^2} - \frac{\partial \ln \Lambda}{\partial s} \frac{\partial}{\partial s} \right) + \frac{\partial^2}{\partial q_3^2} + \frac{\partial \ln(\Lambda \mu)}{\partial q_3} \frac{\partial}{\partial q_3} \quad (16)$$

Here

$$\mu = a(1 + q_3 \kappa_1) \quad (17a)$$

$$\Lambda = \lambda(1 + q_3 \kappa_2) \quad (17b)$$

where κ_1 and κ_2 are the principal curvatures of the tube. The Gaussian curvature K and mean curvature H are defined in terms of the principal curvatures by the relationships

$$K = \kappa_1 \kappa_2 \quad (18a)$$

$$H = \frac{\kappa_1 + \kappa_2}{2} \quad (18b)$$

For our surface parameterizations the principal curvatures are found to be

$$\kappa_1 = \frac{1}{a} \quad (19a)$$

$$\kappa_2 = -\frac{\kappa(s) \cos \theta}{1 - a\kappa(s) \cos \theta} \quad (19b)$$

In the limit $q_3 \rightarrow 0$, the kinetic energy operator reduces to

$$\Delta_t = \frac{1}{a^2} \left(\frac{\partial^2}{\partial \theta^2} + \frac{\partial \ln \lambda}{\partial \theta} \frac{\partial}{\partial \theta} \right) + \frac{1}{\lambda^2} \left(\frac{\partial^2}{\partial s^2} - \frac{\partial \ln \lambda}{\partial s} \frac{\partial}{\partial s} \right) \quad (20)$$

with the distortion potential given by

$$V_D(\theta, s) = -\frac{\hbar^2}{8m^* a^2} \frac{1}{[1 - a\kappa(s) \cos \theta]^2} \quad (21)$$

Thus, for a quantum particle constrained to move on the surface of a tube, the surface Hamiltonian becomes

$$H^{(c)} = -\frac{\hbar^2}{2m^*} \Delta_t + V_D(\theta, s) \quad (22)$$

and

$$H^{(n)} = -\frac{\hbar^2}{2m^*} \frac{\partial^2}{\partial q_3^2} + V(q_3) \quad (23)$$

is the Hamiltonian due to the normal term.

3. The Model

The distorted parts of nanostructures often occur over relatively small sections of the object, so as a first step we choose to model a finite tube with pronounced curvature only over a small region with hard wall boundary conditions at each end. Further simplification follows if we are able to explicitly parameterize by the arclength. As will be seen in the next section, this will facilitate performing the large number of integrations that must be carried out when computing the Gram-Schmidt coefficients and the surface Hamiltonian matrix elements. With this in mind, we choose as our shape function

$$f(u) = -\frac{1}{\kappa_0} \cosh \kappa_0(u - u_0) \quad (24)$$

where κ_0 is the curvature parameter and u_0 is the turning point of the shape function along the u coordinate axis (see Figure 1). The shape function of Eq. (24) has the advantage that the arclength as a function of u is one-to-one and analytically invertible. In terms of arclength, the curvature of the axis is given by

$$\kappa(s) = -\frac{\kappa_0}{1 + [\kappa_0(s - s_0)]^2} \quad (25)$$

where s_0 is the turning point along the arclength. Thus κ_0 is the magnitude of the curvature of the axis at the turning point.

As a crude model of atomic sites of the nanotube or as model of defects of a quantum waveguide, we add periodic δ -function site potentials to the Hamiltonian

$$V(\theta, s) = -\Lambda_0 \sum_{j=1}^{N_a} \sum_{k=1}^{N_r} \delta(\theta - \theta_{jk}) \delta(s - s_k) \quad (26)$$

where Λ_0 is the strength of the potential, θ_{jk} is the value of the angle at the j th site on the k th ring, and s_k is the value of the arclength at the k th ring. N_a and N_r are the number of angular sites per ring and the number of rings, respectively.

4. Solution Method and Results

There are many techniques at our disposal for arriving at the eigenvectors and eigenvalues of curved nanostructures. In a recent work [22], the eigenstates of a quantum particle constrained to move on the surface of a torus were found using a power series technique. That

procedure could be adopted in [22] for two reasons, both of which are consequences of a high degree of symmetry. First, the distortion potential was only dependent upon one coordinate. Secondly, the kinetic energy operator was separable. However, those symmetries are not at play here; the distortion potential is a function of both coordinates and the kinetic energy operator is not separable. Thus, an alternative method must be employed. The alternative chosen here is a basis set expansion.

The main difficulty faced when trying to expand Ψ in a complete set is that, to our knowledge, there is no known set of functions $\{\varphi_k\}$ orthogonal over Σ , i.e., where

$$\int_{\Sigma} \sigma_1 \sigma_2 \varphi_j^*(\theta, s) \varphi_k(\theta, s) = \delta_{jk} \quad (27)$$

holds true. To overcome this difficulty, we make use of the Gram-Schmidt procedure [23] extended to two dimensions. We choose as our original basis the set of $(2M + 1)N$ functions

$$\xi_j(\theta, s) \equiv \xi_{mn}(\theta, s) = e^{im\theta} \sin \frac{n\pi s}{L}$$

where L is the length of the tube, $m = -M, \dots, -1, 0, 1, \dots, M$, $n = 1, \dots, N$, and $|j = 1\rangle \equiv |m = -M, n = 1\rangle$, $|j = 2\rangle \equiv |m = -M + 1, n = 1\rangle, \dots$, $|j = (2M + 1)N\rangle \equiv |m = M, n = N\rangle$. The orthonormal set $\{\varphi_j\}$ is constructed from the non-orthogonal set $\{\xi_j\}$.

Since we have a legitimate basis, the algorithm is straightforward. The Schrodinger equation is solved as a matrix eigenvector-eigenvalue equation with the eigenvectors being the coefficients of the expansion and the elements of the Hamiltonian matrix are defined by

$$H_{jk}^{(c)} = \int_{\Sigma} \sigma_1 \sigma_2 \varphi_j^*(\theta, s) H^{(c)} \varphi_k(\theta, s) \quad (28)$$

Since the Hamiltonian in Eq. (22) is invariant under $\theta \rightarrow -\theta$ we expect the solutions to segregate themselves into positive and negative parity solutions. This will prove useful as a check on the reliability of the numerical results. It should also be noted that in the presence of delta functions, we expect the number of angular peaks in the ground state probability density to be equal to the number of delta sites per ring. This will also serve as a useful check on the numerics.

Using $m^* = m_e$ the $\varepsilon < 0$ results for the tubular arc without delta function site potentials are presented in tables 1-4. As can be seen, all $\varepsilon < 0$, i.e. $m = 0$ states, are of positive parity. The $|m| > 0$ states alternate between positive and negative parity. Table 1 shows the results for the ground state of tubes with several curvature parameters and turning points. Convergence was achieved with 5-digit accuracy using a 20-state ($M = 2, N = 4$) basis set expansion. When $\kappa_0 = 0$, the tube is straight and the system can be solved analytically; the distortion potential is a constant that can be subtracted from the eigenvalues but is left here

for comparison with the arc. It can be seen that the energy of the ground state is lowered when the value of the curvature parameter is increased. However, curvature has little effect on the energies of the excited states (tables 2-4). It should also be noted that the energy of the ground and excited states are sensitive to the position of the bend as well. If the turning point is closer to either end of the tube than it is to $L/2$, the eigenenergies of the ground, first and third excited states are again lowered, however, the energy of the second excited state is raised.

Curvature and bend locations have an effect on the charge (probability) density as well. Although the charge density of the straight tube is angular independent, curvature induces angular dependence in the charge density of the ground state that is maximum at the point of minimum radius of curvature ($\theta = \pi, s = s_0$), i.e. the point of maximum curvature. The charge density of the ground state at $\theta = \pi$ is shown in Figure 2. There is no angular dependence in the excited states, but curvature and bend location still have an effect on the charge density. The nodes and peaks of the density are shifted and the height of the peaks are no longer even (Figs. 3-5).

The eigenvalues of the arc with 1170 ($N_a = 6, N_r = 195$) delta function potentials arranged in an armchair configuration are given in table 5. These results were obtained with a 52-state ($M = 6, N = 4$) expansion. The value for the strength of the potential was chosen to be of the same order of magnitude as the deepest part of the distortion potential well. As can be seen, the ground state is more sensitive to the curvature than the excited states. The slight increase in energy for the third excited states shown in the table may be due to a need for more basis states in the expansion. In the presence of the delta function potentials, charge localization still occurs in the region of curvature (Figure 6); however, there are several islands of localization, with the maximum occurring near the center of the potential well. As expected, the number of islands is equal to the number of delta function sites in each ring, i.e., if there are 6 deltas per ring, there are 6 peaks.

5. Conclusion

The eigenstates and eigenvalues of a particle constrained to move on the surface of a tubular arc with and without delta function sites were computed for several values of κ_0 and s_0 . It was shown that the energy and density were not only sensitive to the strength of the curvature but also to the location of the bend. There was strong interplay between the curvature and delta function potentials demonstrated by the density plot of Figure 6. Charge gets localized by the deltas as well as curvature. The density is still peaked over $s = s_0$, but the maximum peak is no longer at $\theta = \pi$, the center of the well. This peak is slightly displaced due the deltas competing with the curvature as well as each other. What this type of interplay would mean for electron transport is an open question and a topic currently under investigation.

Acknowledgements

L.M. would like to acknowledge useful suggestions from Ms. Samantha Long. L.M. and M.E. received support from NASA Grant No. NAG2-1439.

References

1. H. Jensen and H. Koppe, *Ann. of Phys.* **63**, 586 (1971).
2. R. C. T. da Costa, *Phys. Rev. A* **23**, 1982 (1981).
3. R. C. T. da Costa, *Phys. Rev. A* **25**, 2893 (1982).
4. P. Exner and P. Seba, *J. Math. Phys.* **30**, 2574 (1989).
5. P. Duclos and P. Exner, *Rev. in Math. Phys.*, **7**, 73 (1995).
6. J.T. Londergan, J.P. Carini, D.P. Murdock, *Binding and Scattering in Two Dimensional Systems; Applications to Quantum Wires, Waveguides, and Photonic crystals*, (Springer-Verlag Berlin, 1999).
7. S. Matsutani, *J. Phys. Soc. Jap.* **61**, 55 (1991).
8. J. Goldstone and R. L. Jaffe, *Phys. Rev. B* **45**, 14100 (1991).
9. P. Ouyang, V. Mohta and R. L. Jaffe, *Ann. of Phys.* **275**, 297 (1998).
10. S. Midgley, *Aus. J. Phys* **53**, 77 (2000).
11. S. Midgley and J.B. Wang, *Aus. J. Phys.*, **53**, 77 (2000).
12. I. J. Clark and A. J. Bracken, *J. Phys. A* **29**, 4527 (1996).
13. M. Encinosa and B. Etemadi, *Phys. Rev. A* **58**, 77 (1998).
14. M. Encinosa and B. Etemadi, *Physica B* **266**, 361 (1998).
15. M. Encinosa, *IEEE Trans. Elec. Dev.*, **47**, 878 (2000).
16. R. Saito, G. Dresselhaus, and M.S. Dresselhaus, *Physical Properties of Carbon Nanotubes*, (Imperial College Press, London, 1998).
17. H.R. Shea, R. Martel, and Ph. Avouris, *Phys. Rev. Lett.* **84**, 4441 (2000).
18. S. Matsutani, *Phys. Rev. A* **91**, 686 (1993).
19. S. Matsutani, *J. Phys. A* **30**, 4019 (1997).
20. M. Burgess and B. Jensen, *Phys. Rev. A* **48**, 1861 (1993).
21. H. Flanders, *Differential Forms with Applications to the Physical Sciences*, (Dover Publications, 1989).
22. M. Encinosa and L. Mott, *Phys. Rev. A* **58**, 014102 (2003).

23. G. Arfken and H. Weber, *Mathematical Methods for Physicists*, 5th ed., (Academic Press, New York, 1995).

Table 1: Ground state eigenfunctions and eigenvalues for the tubular arc without delta function site potentials. For all tubes considered here $a = 0.85nm, L = 100nm$. Coefficients not listed are at least an order of magnitude smaller than those given.

κ_0	s_0	$\Psi_{mn}; a = 0.85nm, L = 100nm$	$\varepsilon(meV)$
0.00	—	$\Psi_{01} = .0612 \sin(\frac{\pi s}{100})$	-13.1423
0.75	51.87	$\Psi_{01} = -.0022 \cos \theta \sin(\frac{\pi s}{100}) + .0555 \sin(\frac{\pi s}{100}) - .0042 \sin(\frac{\pi s}{50})$ $+ .0021 \cos \theta \sin(\frac{3\pi s}{100}) - .0253 \sin(\frac{3\pi s}{100}) + .0040 \sin(\frac{\pi s}{25})$	-13.4068
0.75	55.60	$\Psi_{01} = .0023 \cos \theta \sin(\frac{\pi s}{100}) - .0541 \sin(\frac{\pi s}{100}) - .0135 \sin(\frac{\pi s}{50})$ $- .0019 \cos \theta \sin(\frac{3\pi s}{100}) + .0227 \sin(\frac{3\pi s}{100}) + .0014 \cos \theta \sin(\frac{\pi s}{25}) - .0117 \sin(\frac{\pi s}{25})$	-13.4262
0.95	52.37	$\Psi_{01} = .0026 \cos \theta \sin(\frac{\pi s}{100}) - .0526 \sin(\frac{\pi s}{100}) + .0061 \sin(\frac{\pi s}{50})$ $- .0024 \cos \theta \sin(\frac{3\pi s}{100}) + .0302 \sin(\frac{3\pi s}{100}) - .0066 \sin(\frac{\pi s}{25})$	-13.5793
0.95	57.08	$\Psi_{01} = -.0027 \cos \theta \sin(\frac{\pi s}{100}) + .0500 \sin(\frac{\pi s}{100}) + .0012 \cos \theta \sin(\frac{\pi s}{50})$ $- .0179 \sin(\frac{\pi s}{50}) + .0021 \cos \theta \sin(\frac{3\pi s}{100}) - .0248 \sin(\frac{3\pi s}{100}) - .0020 \cos \theta \sin(\frac{\pi s}{25})$ $+ .0183 \sin(\frac{\pi s}{25})$	-13.6313
1.00	52.50	$\Psi_{01} = .0027 \cos \theta \sin(\frac{\pi s}{100}) - .0517 \sin(\frac{\pi s}{100}) + .0065 \sin(\frac{\pi s}{50})$ $- .0025 \cos \theta \sin(\frac{3\pi s}{100}) + .0315 \sin(\frac{3\pi s}{100}) - .0074 \sin(\frac{\pi s}{25})$	-13.6522
1.00	57.45	$\Psi_{01} = -.0028 \cos \theta \sin(\frac{\pi s}{100}) + .0488 \sin(\frac{\pi s}{100}) + .0013 \cos \theta \sin(\frac{\pi s}{50})$ $- .0189 \sin(\frac{\pi s}{50}) + .0021 \cos \theta \sin(\frac{3\pi s}{100}) - .0250 \sin(\frac{3\pi s}{100}) - .0022 \cos \theta \sin(\frac{\pi s}{25})$ $+ .0202 \sin(\frac{\pi s}{25})$	-13.7191
1.15	73.79	$\Psi_{02} = .0027 \cos \theta \sin(\frac{\pi s}{100}) - .0356 \sin(\frac{\pi s}{100}) - .0036 \cos \theta \sin(\frac{\pi s}{50})$ $+ .0438 \sin(\frac{\pi s}{50}) + .0022 \cos \theta \sin(\frac{3\pi s}{100}) - .0235 \sin(\frac{3\pi s}{100}) - .0048 \sin(\frac{\pi s}{25})$	-14.2313

Table 2: Eigenfunctions and eigenvalues of the first excited states of the tubular arc. Coefficients not listed are at least an order of magnitude smaller than those given.

κ_0	s_0	$\Psi_{mn}; a = 0.85nm, L = 100nm$	$\varepsilon(meV)$
0.00	—	$\Psi_{02} = .0612 \sin(\frac{\pi s}{50})$	-13.0296
0.75	51.87	$\Psi_{02} = .0067 \sin(\frac{\pi s}{100}) + .0606 \sin(\frac{\pi s}{50}) + .0045 \sin(\frac{3\pi s}{100})$	-13.0308
0.75	55.60	$\Psi_{02} = .0185 \sin(\frac{\pi s}{100}) + .0577 \sin(\frac{\pi s}{50}) + .0084 \sin(\frac{3\pi s}{100}) - .0025 \sin(\frac{\pi s}{25})$	-13.043
0.95	52.37	$\Psi_{02} = .0103 \sin(\frac{\pi s}{100}) + .0600 \sin(\frac{\pi s}{50}) + .0061 \sin(\frac{3\pi s}{100})$	-13.0308
0.95	57.08	$\Psi_{02} = .0257 \sin(\frac{\pi s}{100}) + .0545 \sin(\frac{\pi s}{50}) + .0098 \sin(\frac{3\pi s}{100}) - .0038 \sin(\frac{\pi s}{25})$	-13.0476
1.00	52.50	$\Psi_{02} = -.0114 \sin(\frac{\pi s}{100}) - .0597 \sin(\frac{\pi s}{50}) - .0067 \sin(\frac{3\pi s}{100}) - .0011 \sin(\frac{\pi s}{25})$	-13.0312
1.00	57.45	$\Psi_{02} = -.0275 \sin(\frac{\pi s}{100}) - .0536 \sin(\frac{\pi s}{50}) - .0100 \sin(\frac{3\pi s}{100}) + .0041 \sin(\frac{\pi s}{25})$	-13.0497
1.15	73.79	$\Psi_{01} = .0488 \sin(\frac{\pi s}{100}) + .0365 \sin(\frac{\pi s}{50}) - .0057 \sin(\frac{3\pi s}{100}) - .0012 \sin(\frac{\pi s}{25})$	-13.1016

Table 3: Eigenfunctions and eigenvalues of the second excited states of the tubular arc. Coefficients not listed are at least an order of magnitude smaller than those given.

κ_0	s_0	$\Psi_{mn}; a = 0.85nm, L = 100nm$	$\varepsilon(meV)$
0.00	—	$\Psi_{03} = .0612 \sin(\frac{3\pi s}{100})$	-12.8416
0.75	51.87	$\Psi_{03} = .0249 \sin(\frac{\pi s}{100}) - .0068 \sin(\frac{\pi s}{50}) + .0554 \sin(\frac{3\pi s}{100}) - .0035 \sin(\frac{\pi s}{25})$	-12.9331
0.75	55.60	$\Psi_{03} = -.0211 \sin(\frac{\pi s}{100}) + .0151 \sin(\frac{\pi s}{50}) - .0546 \sin(\frac{3\pi s}{100}) + .0093 \sin(\frac{\pi s}{25})$	-12.9169
0.95	52.37	$\Psi_{03} = -.0295 \sin(\frac{\pi s}{100}) + .0103 \sin(\frac{\pi s}{50}) - .0524 \sin(\frac{3\pi s}{100}) + .0049 \sin(\frac{\pi s}{25})$	-12.9478
0.95	57.08	$\Psi_{03} = -.0225 \sin(\frac{\pi s}{100}) + .0208 \sin(\frac{\pi s}{50}) - .0516 \sin(\frac{3\pi s}{100}) + .0012 \sin(\frac{\pi s}{25})$	-12.9182
1.00	52.50	$\Psi_{03} = .0306 \sin(\frac{\pi s}{100}) - .0115 \sin(\frac{\pi s}{50}) + .0514 \sin(\frac{3\pi s}{100}) - .0053 \sin(\frac{\pi s}{25})$	-12.9515
1.00	57.45	$\Psi_{03} = -.0227 \sin(\frac{\pi s}{100}) + .0221 \sin(\frac{\pi s}{50}) - .0508 \sin(\frac{3\pi s}{100}) + .0013 \sin(\frac{\pi s}{25})$	-12.9178
1.15	73.79	$\Psi_{03} = -.0100 \sin(\frac{\pi s}{100}) + .0222 \sin(\frac{\pi s}{50}) + .0559 \sin(\frac{3\pi s}{100}) + .0041 \sin(\frac{\pi s}{25})$	-12.874

Table 4: Eigenfunctions and eigenvalues of the third excited states of the tubular arc. Coefficients not listed are at least an order of magnitude smaller than those given.

κ_0	s_0	$\Psi_{mn}; a = 0.85nm, L = 100nm$	$\varepsilon(meV)$
0.00	—	$\Psi_{04} = .0612 \sin(\frac{\pi s}{25})$	-12.5784
0.75	51.87	$\Psi_{04} = -.0022 \sin(\frac{\pi s}{100}) + .0048 \sin(\frac{3\pi s}{100}) + .0610 \sin(\frac{\pi s}{25})$	-12.5799
0.75	55.60	$\Psi_{04} = .0065 \sin(\frac{\pi s}{100}) - .0027 \sin(\frac{\pi s}{50}) - .0133 \sin(\frac{3\pi s}{100}) - .0593 \sin(\frac{\pi s}{25})$	-12.6136
0.95	52.37	$\Psi_{04} = .0034 \sin(\frac{\pi s}{100}) - .0074 \sin(\frac{3\pi s}{100}) - .0606 \sin(\frac{\pi s}{25})$	-12.5805
0.95	57.08	$\Psi_{04} = .0093 \sin(\frac{\pi s}{100}) - .0049 \sin(\frac{\pi s}{50}) - .0194 \sin(\frac{3\pi s}{100}) - .0571 \sin(\frac{\pi s}{25})$	-12.6398
1.00	52.50	$\Psi_{04} = .0038 \sin(\frac{\pi s}{100}) + .0013 \sin(\frac{\pi s}{50}) - .0083 \sin(\frac{3\pi s}{100}) - .0605 \sin(\frac{\pi s}{25})$	-12.5804
1.00	57.45	$\Psi_{04} = .0102 \sin(\frac{\pi s}{100}) - .0056 \sin(\frac{\pi s}{50}) - .0211 \sin(\frac{3\pi s}{100}) - .0562 \sin(\frac{\pi s}{25})$	-12.6475
1.15	73.79	$\Psi_{04} = .0012 \sin(\frac{\pi s}{100}) - .0028 \sin(\frac{\pi s}{50}) + .0057 \sin(\frac{3\pi s}{100}) - .0609 \sin(\frac{\pi s}{25})$	-12.25592

Table 5: Eigenvalues of the tubular arc with 1170 ($N_a = 6, N_r = 195$) δ -function site potentials arranged in an armchair configuration with $\Lambda_0 = 400meV \cdot nm$. The subscripts on the eigenvalues are *not* quantum numbers. They refer to the order of the energies: 0 is the ground state; 1 is the first excited state and so on.

κ_0	s_0	$\varepsilon_0(meV)$	$\varepsilon_1(meV)$	$\varepsilon_2(meV)$	$\varepsilon_3(meV)$
0.00	—	-872.208	-872.095	-871.907	-871.643
0.95	52.37	-872.587	-872.115	-872.012	-871.627
1.00	52.50	-872.655	-872.119	-872.018	-871.624

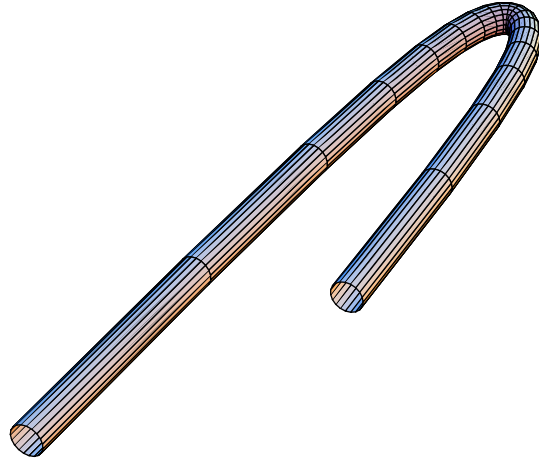


Figure 1: A tubular arc.

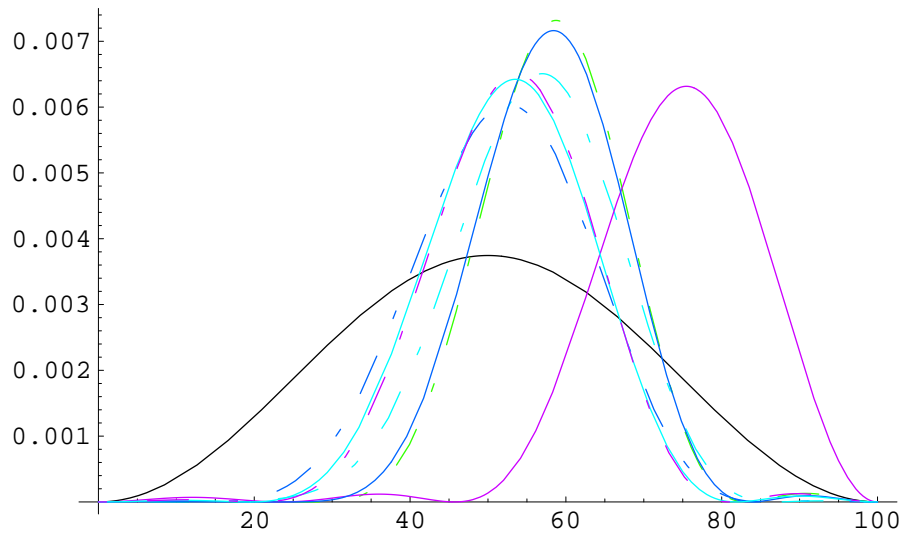


Figure 2: Probability densities of the states given in Table I at $\theta = \pi$. The color code is as follows and is the same for the remaining figures: solid black ($\kappa_0 = 0.00$); dashed blue ($\kappa_0 = 0.75, s_0 = 51.87$); dashed turquoise ($\kappa_0 = 0.75, s_0 = 55.60$); solid turquoise ($\kappa_0 = 0.95, s_0 = 52.37$); solid blue ($\kappa_0 = 0.95, s_0 = 57.08$); dashed pink ($\kappa_0 = 1.00, s_0 = 52.50$); dashed green ($\kappa_0 = 1.00, s_0 = 57.45$); solid pink ($\kappa_0 = 1.15, s_0 = 73.79$).

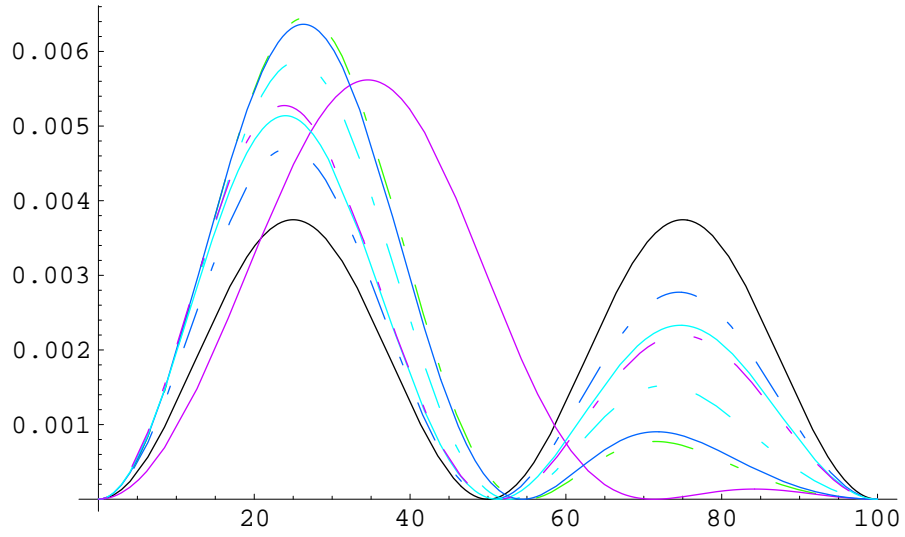


Figure 3: Probability densities of the states given in Table II at $\theta = \pi$.

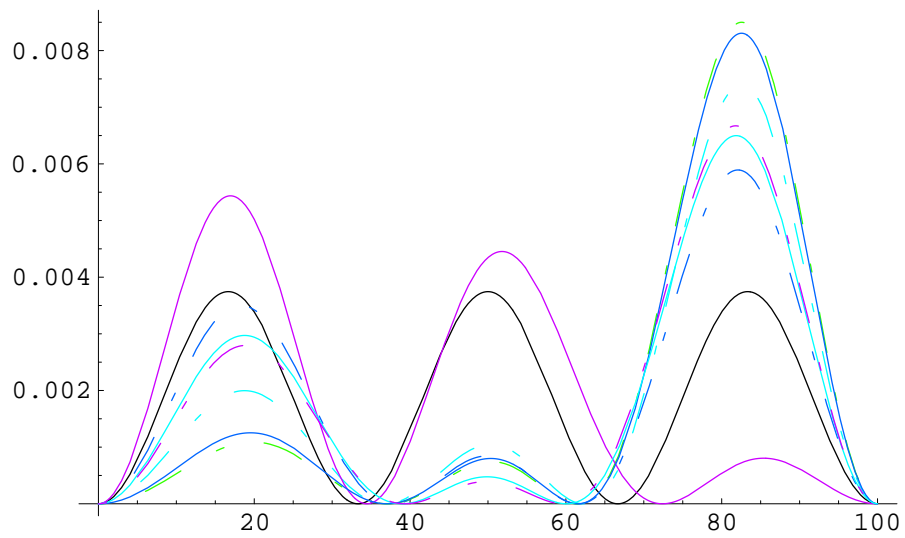


Figure 4: Probability densities of the states given in Table III at $\theta = \pi$.

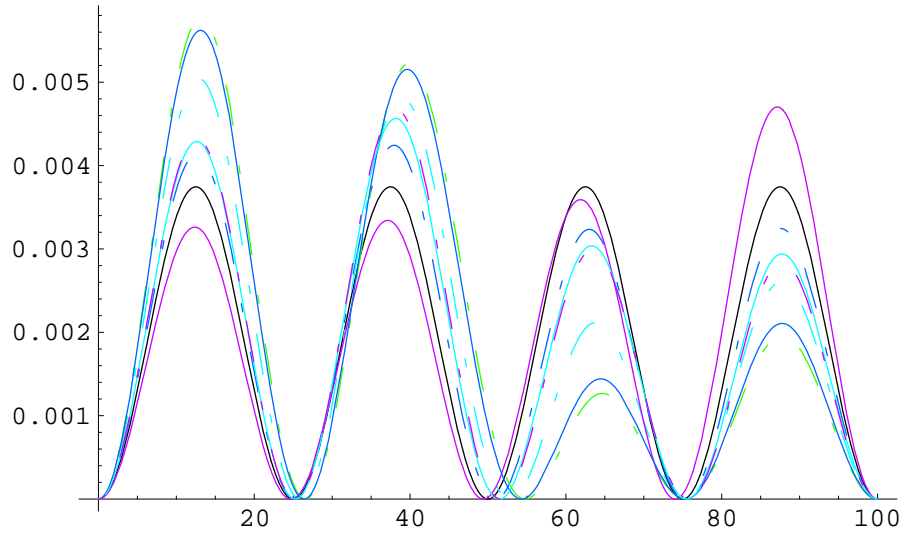


Figure 5: Probability densities of the states given in Table IV at $\theta = \pi$.

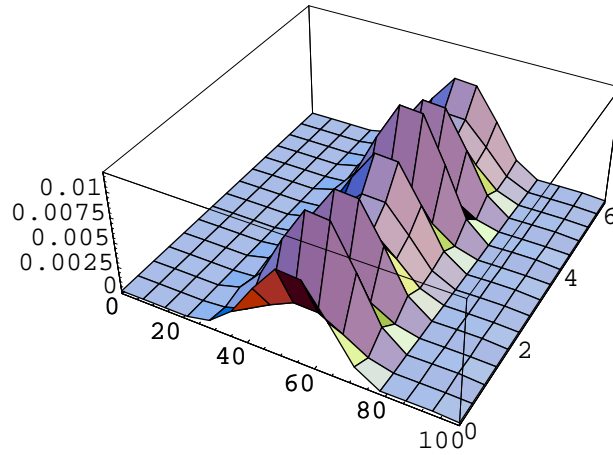


Figure 6: Probability density of the ground state of a tubular arc ($\kappa_0 = 1.00, s_0 = 57.45$) with delta function site potentials.